

Optical Properties of Si Quantum Dots in Silica via an Implantation Mask

Eric G. Barbagiovanni, Lyudmila V. Goncharova, P. J. Simpson and Nathan Armstrong
Department of Physics and Astronomy, The University of Western Ontario, London, Ontario,
Canada, N6A 3K7

ABSTRACT

We studied photoluminescent properties and luminescent decay dynamics in Si quantum dots (QDs) produced by Si implantation in SiO₂, and their modification by the application of an implantation mask. Silicon quantum dots were prepared by ion implantation, followed by high temperature annealing leading to nanocrystal nucleation and growth. The mask was prepared by spin-coating silica microspheres to achieve laterally-selective implantation, to control QD size and separation. Transmission electron microscopy (TEM) images were obtained to verify the diameter of the quantum dots. We observe a noticeable peak shift and narrowing in the photoluminescence spectra with the application of the implantation mask. Observed maxima in the photoluminescence spectra are compared with a quantum field theoretical model using an infinite confining 1D potential for Si quantum dots. We comment on the role of excitation transfer by observing a change in the dispersion exponent of the luminescent decay dynamics due to the mask.

INTRODUCTION

Considerable effort has been spent in investigating the structural, electronic and optical properties of silicon nanostructures. In particular, low dimensional structures with silicon quantum dots embedded in an SiO₂ matrix have drawn much attention due to their interesting luminescent properties and their compatibility with standard silicon processing technologies, such as implantation and thermal treatments.

Quantum dots (QDs) produced by ion implantation are primarily controlled by a few parameters: implantation dose, implantation energy and annealing conditions [1]. In addition, implantation geometry, pre-implantations to create disorder, multiple implant conditions and temperature during implantation can be considered. The annealing conditions also determine the size of the QDs [2]. In the first moments of annealing (<100s) nucleation sites are created, followed by Ostwald ripening [3]. Implantation through a mask provides control over the lateral distribution of implanted ions. A mask with openings on the order of a desired QD diameter should make possible an ordered array of uniformly-sized QDs with controlled spacing and to investigate the mechanisms of excitation transfer between QDs. A reduced size (in the quantum confinement limit) and narrow size distribution of QDs, will cause changes in the characteristic photoluminescent properties [4,5]. Various technologies benefit from the desired increase in parameter control [6,7,8].

Work, thus far, on Si QDs has been directed primarily on the origin of the luminescence spectrum, e.g., whether it is due to quantum confinement (red emission) or defect related (blue emission), with lifetimes of ~20-100μs reported for quantum confined systems [9,10]. In this work, a mask is used to isolate QDs to study individual QD radiative processes. Although the work is still in progress to achieve the desired mask feature size of ~10 nm, here we show the impact of larger mask sizes on the optical properties of QDs. We show a reduction in QD size/

distribution investigated with photoluminescence measurements. In addition, we report on a proposed model for excitation transfer by studying the decay dynamics observing a reduction of radiative mechanisms between QDs in masked samples.

EXPERIMENT

We used a mask of close-packed SiO₂ micro-spheres (SiO₂-ms, Kisker-Biotech) one mono-layer thick, of diameters 100nm, 400nm, 800nm and 1000nm. SiO₂-ms were chosen over polystyrene-latex micro-spheres because the former do not deteriorate during the implantation process [11]. Secondary electron micrographs (SEM) were taken after the implantation to inspect the mask and to verify that there is no macroscopic damage imparted to the SiO₂-ms.

Substrates of Si (100) with 135nm of thermally grown oxide were masked by spin-coating. Prior to spin-coating, the substrate was made hydrophilic by placing it in an ultrasonic bath of acetone followed by de-ionized water (DI-H₂O) for an hour each, as described in [12]. After the ultrasonic bath, the substrates were stored in DI-H₂O until they were ready to be used.

A 95% solution of SiO₂-ms in DI-H₂O was diluted with methanol at a volumetric ratio of 200:1 to allow wetting of the surface and to obtain a close-packed mask one monolayer thick. Just before spinning, the substrates were removed from the DI-H₂O and placed on a hot plate (T≈100°C). The heating helped to obtain a close-packed arrangement [12]. 0.1ml of the above-mentioned solution was placed on the substrate and spun at 100 rpm for 30s. The speed was then lowered to 50 rpm until dry. Samples were created using the four different SiO₂-ms sizes along

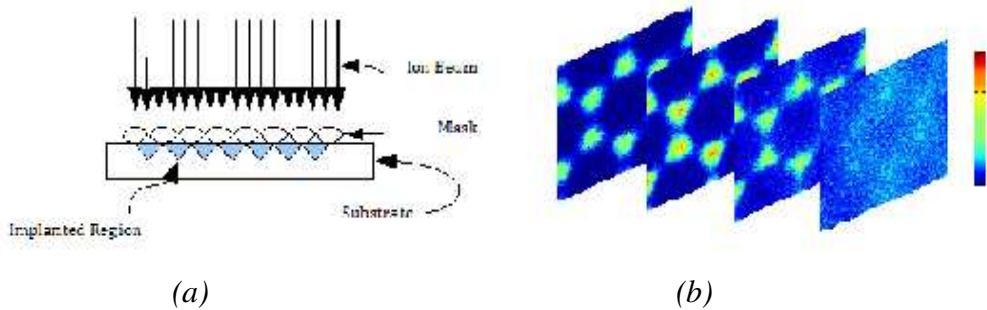


Figure 1. *a: Schematic of ion implantation with a SiO₂-micro-spheres mask. b: Simulation of the Si implant profile in SiO₂ with depth sectioned at 8, 16, 24 and 32nm (from left to the right).* with a reference sample using no mask.

Si ions were implanted through the micro-sphere mask creating a discrete matrix of implanted regions, represented in figure 1a. The implantation conditions were 25keV Si⁺ ions at a dose of 4×10^{16} ions/cm², 10^{-7} Torr, 40μA over an area of 10cm², at room temperature and normal incidence. The projected range R_p predicted by Stopping and Range of Ions in Matter (SRIM) [13] is 40nm, sufficiently low to ensure that the implanted ions would not penetrate the full chord of the smallest mask size. To predict the 3D distribution of implanted ions within the substrate, simulations were performed using SRIM combined with the lateral mask footprint (shown in figure 1b).

After ion implantation, the samples were cleaned with an acetone wipe to remove the mask. The samples were then annealed at 1100°C for 15 min in a N₂ environment (Jipelec JetFirst rapid thermal annealer). This step created nucleation sites followed by Ostwald ripening, and with the mask in place we expect smaller QDs and a narrower distribution of sizes than

without a mask by reducing the number of nucleation sites [14]. Afterwards, the samples were heated in a furnace at 500°C for 1hr in a 95% N₂/ 5%H₂ environment to eliminate dangling bonds; thereby, increasing the efficiency of the luminescence process [15].

RESULTS AND DISCUSSION

As a diagnostic for the mask's ability to control the lateral distribution of implanted ions, we implanted masked samples with 25keV Au⁺ at room temperature. Christiansen et al. have shown that low-energy implanted Au atoms rise to the surface after annealing and can therefore be used to show the pattern of masked implantation [16]. After the same annealing procedure as [16], SEM images showed that Au was confined to the regions of the surface exposed between the masking spheres.

The micrographs of figure 2 show the results of the spin coating process for the 1000nm and 100nm SiO₂-ms. For an ideal monolayer close-packed SiO₂-ms coverage, only 10% of surface area would be exposed and implanted with Si. This number has to be adjusted due to imperfections in the spin-coating process. Micrographs such as figure 2, were used to calculate the experimental percent coverage (using the Image J software), defined as 100% x (total area - SiO₂-ms free area)/total area. The measured coverage was 79% for both 1000nm and 800 nm spheres, 73% for 400nm and 88% for 100nm, each over a 1mm² sample area (chosen to be consistent with the PL laser diameter). Percent coverage was factored into the surface area calculation to determine the reduction in intensity of the PL signal, discussed below.

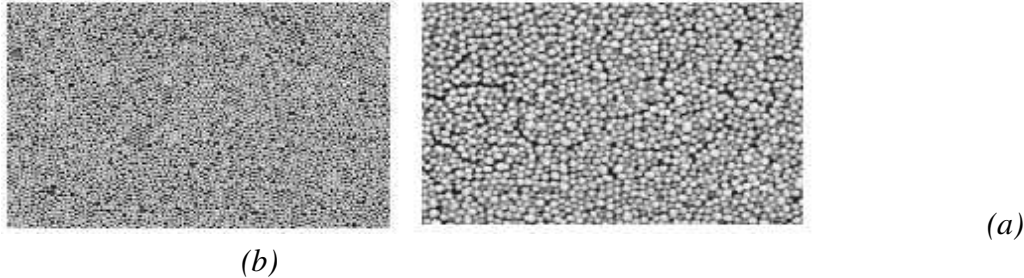


Figure 2. Scanning electron micrographs of 3a: 1000nm, 3b: 100nm SiO₂-ms atop SiO₂ substrates after spin coating.

Transmission electron microscopy (TEM) imaging was performed to verify the morphology, distribution and diameter of the Si QDs using a FEI Titan 80-300 operated at 300 kV. The average diameter given by the TEM measurements is 1.76±0.64nm. A sample TEM image is given in figure 3. The resolution of the imaging was not sufficient to observe any

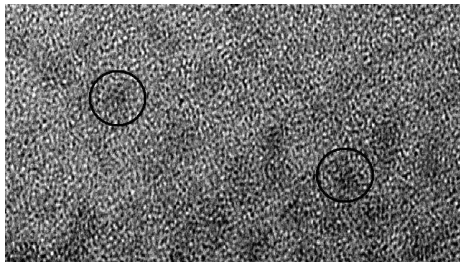


Figure 3. Transmission electron microscopy (TEM) image of Si QDs in SiO₂. Circles highlight representative QDs.

change in QD size from the masked to the unmasked sample.

Photoluminescence (PL) measurements were performed at room temperature with a 325nm laser at 17mW, and an effective power density of 0.64 W/cm². Light emission was analyzed by an Ocean Optics spectrometer with 600 gratings/mm, resulting in a large spectral window of 350-1000nm. Several PL measurements were made for each sample. Each subsequent measurement was taken \approx 1mm from the previous measurement, labeled accordingly as '1', '2', '3' or '4', while 'no mask' was the reference sample, in figure 4. We did not observe a significant difference between mask sizes, but there is a clear difference between masked and unmasked samples.

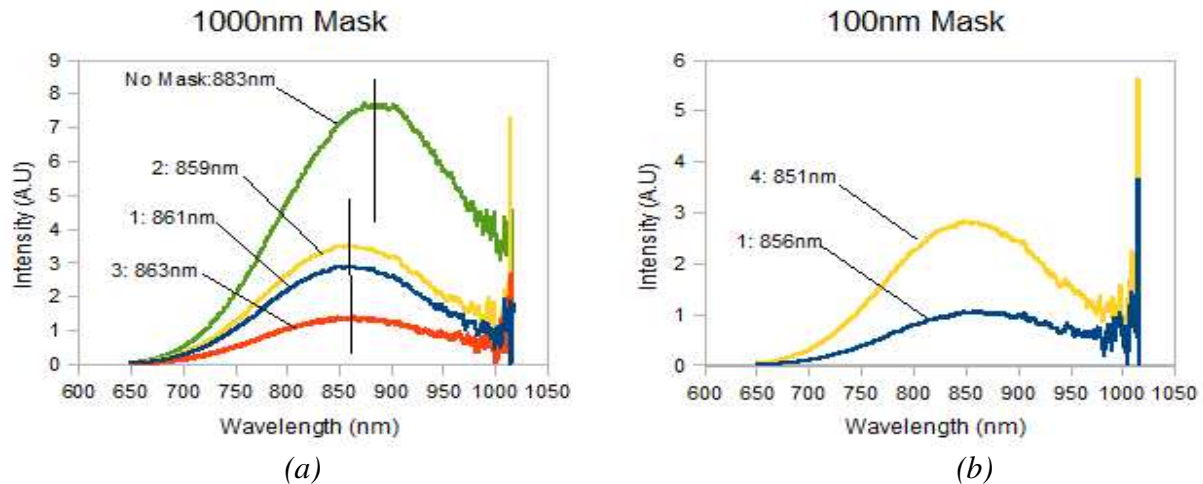


Figure 4. Photoluminescence spectra of Si QDs in SiO₂. SiO₂-ms mask sizes- 4a: 1000nm, 4b: 100nm. '1', '2', '3', '4' labels represent sample measurements taken 1mm apart. 'No Mask' labels the reference sample. Peak maximum wavelengths indicated for each curve. Several curves were omitted for clarity. Wavelength markers shown in 4a highlight shift in peak wavelength.

There were three central observations (figure 4), which represent the effect of the mask. The first striking feature was the shift in the peak wavelength. The peak wavelength maximum for the reference ('no mask') sample was 883nm. There was an observed shift for all the samples with the mask to an average wavelength of 840nm. There was an apparent correlation between the % coverage and the peak position in the PL spectrum: where there was reduced PL intensity, presumably due to greater % coverage, the PL curves shifted toward the blue. This shift in wavelength was assumed to represent a reduction in the average size of QDs produced, independent of the mask size, due to quantum confinement for which $E \propto 1/r^2$.

The second observation was the narrowing of the width of the peak in the PL spectrum for all samples with a mask. The full width half maximum (FWHM) due to the mask in figure 4 is 182 ± 9 nm, while the 'no mask' curve has a FWHM of 213nm. This observation suggests that there was a reduction in the distribution of the QD sizes due to the mask with the assumption that each wavelength of the PL spectrum relates to a particular diameter of QD. The distribution of sizes is discussed in more detail below.

The final feature was the intensity of the light emission. The predicted intensity due to the reduction in implanted area, from the reference sample with an intensity of 7.6, yields for 1000nm and 800nm \approx 2.4, for 400nm \approx 2.8 and for 100nm \approx 1.7. These numbers agree quantitatively with the observed PL intensities.

To relate the diameter of the QDs to the luminescent emission energy, we calculated the energy spectrum of a two band model and fit this result with the peak emission wavelength obtained from the PL data, to yield the diameter of the QDs. Calculations were performed using a quantum field theoretical model with an infinite confining 1D potential, while ignoring the exchange term. All wave functions were given by plane waves expanded over Bloch states. Calculations were performed near the band edge, expanding in the limit $k \rightarrow 0$. For the reference sample the peak emission energy was 1.4eV (883nm), from which we calculate a diameter of 1.78nm, which is in fair agreement with the diameters obtained via TEM. For a masked sample the peak emission is at 1.48eV (840nm), yielding a QD diameter of 1.57nm. These calculations also agree with data from a range of similar samples [17]. Further, we note that these calculations using 1D confinement fit the experimental data much better than a 3D model does. The reason for this fact is an interesting avenue for further investigation.

Radiative lifetime measurements were performed using a Hamamatsu R7400U-20 photomultiplier tube (PMT). The samples were excited with a 405nm laser with an effective power of 9mW pulsed at 1kHz. The pulse on the laser was used to trigger an oscilloscope (Agilent 3000 series), which records the output signal from the PMT. Lifetime results are shown in figure 5.

These data are modeled using a stretched-exponential law:

$$I=I_0 \exp(-(t/\tau)^\beta) \quad (1)$$

where τ is the lifetime of the QDs and β is the dispersion exponent. We calculate β to be $\beta=0.78\pm0.02$ (1000nm mask) using fitted curve equations presented in Figure 5a, while for the reference sample it is $\beta=0.74\pm0.03$.

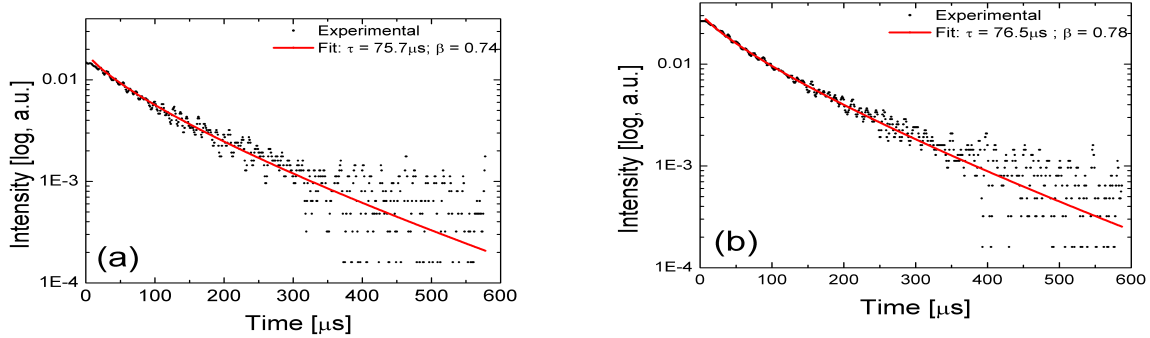


Figure 5. Unnormalized excitation decay for a: Reference sample and b: 1000nm masked sample. Fit is given by equation 1. Lifetime and beta are given in plot.

The role of the mask is to create isolated regions of QDs in the substrate matrix. When QDs are isolated the probability of excitation transfer from one QD to another is reduced. The narrower PL spectrum found for masked samples reflects a narrower QD size distribution. If a small QD is excited, there exists a finite probability that it can excite a larger QD, because the band gap is larger in smaller QDs [18]. If the distribution of QD sizes is narrow, then the probability of excitation transfer is reduced. Thus, it is reasonable to assume the number of radiative events is reduced in a sample with a mask in place [19]. If $\beta=1$, then there exists a single decay mechanism. For $\beta<1$, multiple decay mechanisms exist. This suggests that the smaller value of β found for the unmasked sample is consistent with our qualitative understanding of the radiative processes.

CONCLUSIONS

We developed a procedure to form a SiO₂-microsphere implantation and investigated effects of the mask on Si QD formation and QD photoluminescent and lifetime characteristics. The masked caused a shift in the PL peak wavelength and a narrowing of the PL spectrum, as well as the expected reduction in the PL intensity due to a reduced density of QDs. The peak wavelength decreases with the mask limiting the growth of QDs. Calculations indicate a reduction in QD diameter by 0.21nm. The application of the mask created discrete regions of QDs, thereby, limiting the role of excitation transfer in the luminescent dynamics. In this work, we demonstrated a reduction in radiative events due to a change in QD size/ distribution by creating discrete regions of QDs. Further work is being conducted to investigate directly the origin of the various (non) radiative processes.

ACKNOWLEDGMENTS

We would like to thank Dr. Andy Knights of McMaster University for valuable discussions and use of lab facilities. We thank Dr. Carmen Andrei and the Canadian Centre for Electron Microscopy for work on the TEM imaging. Partial support of this project from the Natural Sciences and Engineering Research Council (NSERC) of Canada is gratefully acknowledged.

REFERENCES

1. C. R. Mokry, P. J. Simpson, and A. P. Knights., Proceedings SPIE 6343, June 2006. Photonics North 2006, Pierre Mathieu, Editors, 63432P.
2. C. Bonafos, B. Colombeau, A. Altibelli, M. Carrada, G. Ben Assayag, B. Garrido, M. López, A. Pérez-Rodríguez, J. R. Morante, and A. Claverie., Nuc. Instr. and Meth. in Phys. Res. B 178, 17 (2001).
3. A. P. Knights. To be published.
4. C. Delerue, G. Allen, and M. Lannoo., Phys. Rev. B. 48, 11024 (1993).
5. D. J. Lockwood, Z. H. Lu, and J. M. Baribeau., Phys. Rev. Lett. 76, 539 (1996).
6. V. Aroutiounian, S. Petrosyan, A. Khachatryan, and K. Touryan., J. Appl. Phys. 89, 2268 (2001).
7. D. Englund, D. Fattal, E. Waks, G. Solomon, B. Zhang, T. Nakaoka, Y. Arakawa, Y. Yamamoto, and J. Vucković., Phys. Rev. Lett. 95, 013904 (2005).
8. A. Dousse, L. Lanco, J. Suffczyński, E. Semenova, A. Miard, A. Lemaître, I. Sagnes, C. Roblin, J. Bloch, and P. Senellart., Phys. Rev. Lett. 101, 267404 (2008).
9. K. S. Min, K. V. Shcheglov, C. M. Yang, Harry A. Atwater, M. L. Brongersma, and A. Polman., Appl. Phys. Lett. 69, 2033 (1996).
10. P. Mutti, G. Ghislotti, S. Bertoni, L. Bonoldi, G. F. Cerofolini, L. Meda, E. Grilli, and M. Guzzi., Appl. Phys. Lett. 66, 851 (1995).
11. E. Snoeks, A. van Blaaderen, T. van Dillen, C.M. van Kats, K. Velikov, M.L. Brongersma, and A. Polman., Nucl. Instr. and Meth. in Phys. Res. B. 178, 62 (2001).

12. B. T. Chen, V. Ng, and A. O. Adeyeye., Phys. Rev. Lett., pages 71–4, 2001. Nanotechnology, 2001. IEEE-NANO 2001. Proceedings of the 2001 1st IEEE Conference.
13. J. P. Biersack and J. F. Ziegler, 2008. <http://www.srim.org/>.
14. T. S. Iwayama, T. Hama, D. E. Hole, and I. W. Boyd., Vacuum 81, 17985 (2006).
15. M. López, B. Garrido, C. García, P. Pellegrino, A. Pérez-Rodríguez, J. R. Morante, C. Bonafos, M. Carrada, and A. Claverie., Appl. Phys. Lett. 80, 1637 (2002).
16. S. Christiansen, R. Schneider, R. Scholz, U. Gösele, Th. Stelzner, G. Andrä, E. Wendler, and W. Wesch., J. Appl. Phys. 100, 084323 (2006).
17. C. R. Mokry, P. J. Simpson, and A. P. Knights., J. Appl. Phys. 105, 114301 (2009).
18. C. Q. Sun, T. P. Chen, B. K. Tay, S. Li, H. Huang, Y. B. Zhang, L. K. Pan, S. P. Lau, and X. W. Sun., J. Phys. D: Appl. Phys. 34, 3470 (2001).
19. C. Reynaud, O. Guillois, N. Herlin-Boime, G. Ledoux, and F. Huisken, Mater. Res. Soc. Symp. Proc. 832, F6.2.1 (2005).